35. R. Birringer and H. Gleiter, in *Encyclopedia of Materials Science and Engineering*, edited by R. W. Cahn (Pergamon Press, Oxford, 1988), Suppl. Vol. 1, pp. 339–349.

36. D. G. Cahill and R. O. Pohl, Ann. Rev. Phys. Chem. **39**, 93 (1988).

2.B Energy Transport in a Modern Disk Amplifier

The University of Rochester's Laboratory for Laser Energetics has designed, built, and characterized a modern, 20-cm clear aperture, Nd:glass Brewster-disk amplifier. This device will be used as the final amplifier in the upgrade of the existing OMEGA laser system. This article describes results of the energy characterization of that amplifier. Specifically, spatially resolved measurements of small-signal gain and whole-beam measurements of large-signal gain are described. The amplifier met its small-signal-gain design goal of 3.0 at only 70% of the design capacitor-bank energy with adequate spatial uniformity. A storage efficiency of 1.7% was achieved. Large-signal-gain measurements, both with and without 5-Å-FM bandwidth on the extracting beam, display no measurable change in gain because of the impressed bandwidth.

The amplifier is termed modern in that it incorporates a number of improvements suggested by others in the community[1] who have extensive experience in building disk amplifiers, as well as several uniquely new features. A few examples of these improvements include minimization[2] of total amplifier volume for better coupling of flash lamps to laser glass, transversely-pumped rectangular design to avoid obscuration of flash lamps by the disk supports,[3] water-cooled flash lamps,[4] and polymerically-bonded edge cladding.[5]

A brief description of the amplifier follows; the detailed design and construction of the amplifier is described elsewhere.[6,7] A picture of the amplifier with some of its flash lamps removed for clarity is shown in Fig. 49.27. The amplifier consists of four disks of 2-wt% Nd:phosphate glass, 3.0 cm thick. The number of disks was chosen in order to obtain adequate gain at the 3.0-cm thickness. The 3.0-cm thickness and the 550-μs $3\sqrt{LC}$ pump pulse width are optimized for high-gain-per-unit path in glass in order to minimize B-integral. The disks rest on edge, that is, their surface normals lie in a horizontal plane. The amplifier is pumped by 80, 19-mm bore, 10-in. arc length, vertically oriented (transverse), xenon flash lamps. The lamps are mounted on 1.341-in. centers for a packing fraction of 1.75. These lamps are connected in series of five, both electrically and for cooling. Each group (brick) of five lamps is connected to one pulse-forming network (PFN) that can deliver 18.8 kJ of energy at 100% of nominal bank energy. At this bank energy the lamps operate at 26% explosion fraction.

G3250

Fig. 49.27
Picture of the 20-cm-disk amplifier with the near-side flash-lamp modules lowered for clarity. Note the transversely mounted flash lamps.

The characterization of this amplifier proceeded in two phases: energy transport and wavefront. Energy-transport measurements were performed first to determine if the amplifier met design goals for gain and extraction. After it was verified that the amplifier met energy goals, the wavefront was characterized using time-resolved Mach-Zehnder interferometry. Wavefront results will be presented at a later date. Energy-transport measurements included passive loss, small-signal gain, and large-signal gain. Small-signal-gain measurements were made as a function of position in the clear aperture and bank energy to obtain information about the internal dynamics of the amplifier. The large-signal-gain tests were conducted with the anticipated spectral bandwidth for the OMEGA Upgrade because of recent reports[8] of reduced extraction at large incoherent (~25 Å) bandwidths.

Small-Signal Gain

The small-signal gain was measured with the apparatus[9] shown in Fig. 49.28. This apparatus measured the small-signal gain at three locations on a diameter of the aperture (either horizontal or vertical) simultaneously, thus reducing the number of shots required. Typically, the inner beam measured the center-line gain, while the two outer beams were translated across the diameter. A polarized cw Nd:YLF oscillator operating on the 1.054-μm transition was collimated, expanded to a 1-cm diam, and split three ways. Each of the three beams was then injected into the amplifier. A mirror with a small horizontal tilt (<1 mrad) returned the beams back through the amplifier. The small offset (<0.4 cm) between the input and return of the beams on the first disk did not significantly affect the spatial resolution of the measurement. Each return beam was first dispersed by a grating to discriminate against spectrally-near fluorescence. Each beam then reflected from a 1-μm mirror to limit the amount of flash-lamp light reaching the detector. Spatial filters with a 1-mrad full-angle cutoff followed the

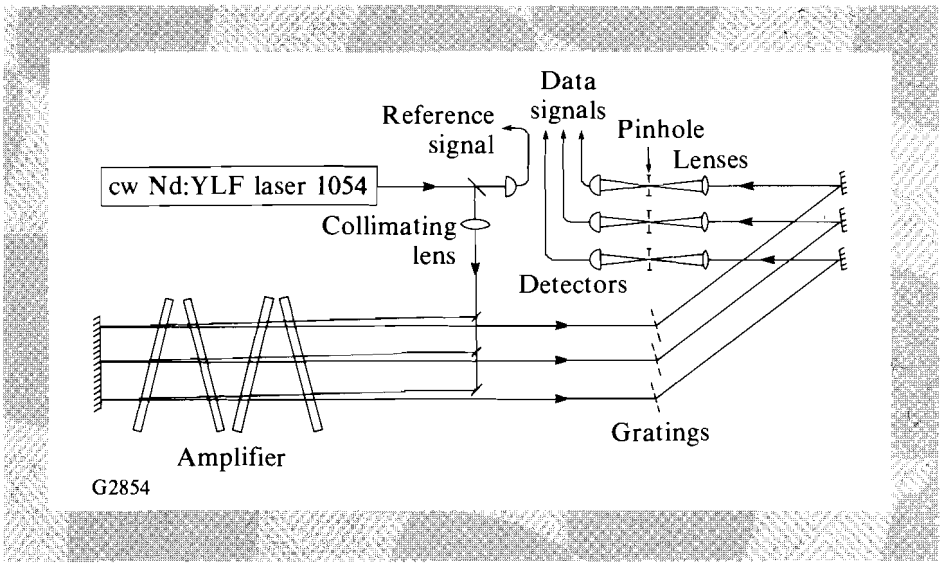

Fig. 49.28
Schematic of the small-signal-gain apparatus. The cw Nd:YLF laser is split into three beams that probe different locations on either a horizontal or vertical diameter in the aperture. The return signals are filtered spectrally with gratings and spatially filtered before detection.

mirrors. Large-area photodiodes with a measured 1/e response time of 2 μs detected the return signals. A fourth identical photodiode monitored the Nd:YLF laser output as a reference channel.

Signals from the large-area photodiodes were digitized by Tektronix[10] 2440 oscilloscopes with a 500-megasample-per-second, maximum-digitizing rate. Signals were digitized into 2-ms, 1024-sample record lengths with 8-bit amplitude resolution. The 2-ms record length ensured that the entire temporal history of the gain and a portion of all signals prior to the initiation of the flash-lamp discharge were recorded. The signals were then Fourier transformed, filtered with a Blackman[11] filter whose cutoff frequency was 100 kHz. Background "shots" were taken at intervals during the measurement. For these shots, the cavity of the Nd:YLF was blocked and all of the signals mentioned previously were recorded. This background included fluorescence from the amplifier and any noncancelling noise. It was determined that the fluorescence part of the signal from the amplifier was negligible and only a DC offset from the detectors was significant. The background offset collected for each channel was subtracted from the data for that channel. The temporal variations of the Nd:YLF were removed by dividing each of the three signal channels by the reference channel. A 200-μs sample of each of the three channels prior to the initiation of the discharge was averaged and set equal to unity gain. The remainder of the data in that channel was multiplied by the so-determined constant to convert the data to gross small-signal gain. The peak gain in the channel was picked with a simple search routine. The estimated precision attained as a result of this procedure is ±1%. A 90-mm-rod amplifier with dedicated pump modules (flash lamps) and diagnosed power conditioning was kept as a control. The gain of this amplifier could be routinely remeasured with ±1% precision.

Initial measurements were of center-line gain versus capacitor-bank energy. The results are plotted in Fig. 49.29. The design goal of 3.0 was achieved at 70% of nominal bank energy. This corresponds to a disk-thickness-averaged, stored-

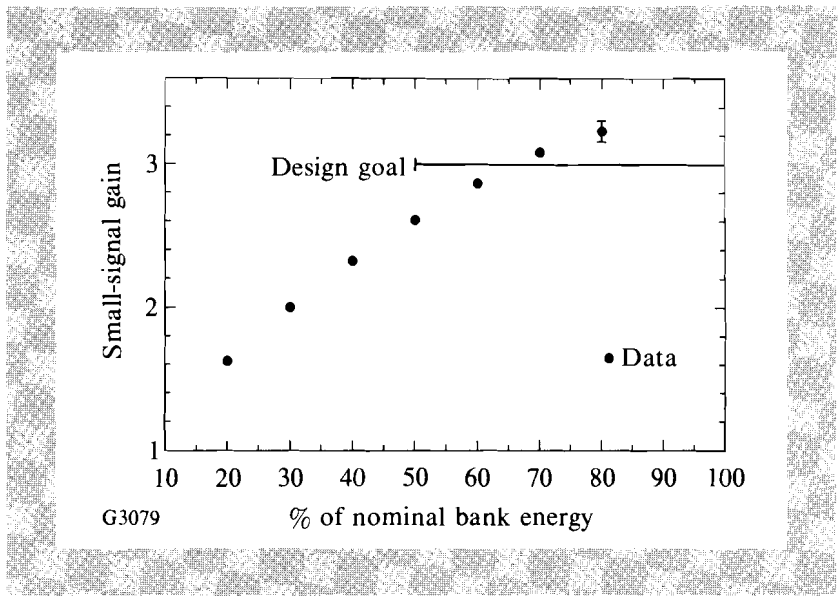

Fig. 49.29
Measured small-signal gain versus the percentage of nominal capacitor-bank energy. The small-signal design goal was achieved at 70% of the design bank energy.

energy density of 0.41 J/cc assuming a stimulated-emission cross section of 3.5×10^{-20} cm^2. The data displays no sharp rollover or plateau that would signify parasitic clamping or severe amplified spontaneous emission (ASE) limiting.[12]

The fact that the gain design goal was achieved at only 70% of "nominal" bank energy provides a margin of safety for both power balance[13] and, more importantly, long-term amplifier performance. Equalization of individual amplifier gains will be necessary in order to maintain instantaneous power balance among the OMEGA Upgrade beamlines. It is a well-known observation that amplifier performance declines with number of shots. Causes of this degradation include effects such as solarization of the laser glass, blast windows, water jackets, etc., reflector tarnishing, and damage caused by inadequate cleanliness in the pump cavity. Simulations show that a 25% reduction in the gain of the amplifier results from a 15% reduction in the reflectivity in the pump cavity. The extra gain margin ensures that this amplifier will perform to specification near end of life (20,000 shots). For all further testing the amplifier was operated just over its gain design goal at 80% of nominal bank. This corresponded to a center-line small-signal gain of 3.22±0.03. This was done to ensure that had any short-term gain decrease occurred, the testing would have been carried out at at least the design gain. The corresponding $\alpha_o \overline{E}_s D$ product for these disks is 2.93 where $\overline{E}_s = 0.44$ J/cm^3 and D is the major diameter of the 20-cm clear aperture projected at Brewster's angle.

The small-signal gain was next measured as a function of position on the horizontal and vertical diameters of the aperture. In order to separate the effects of shot-to-shot gain variations from actual spatial variations, the inner probe beam monitored the center-line gain while only the outer two probe beams were translated along the diameters. Outer probe-beam data from different shots were normalized by comparing the center-line gains. The shot-to-shot variation in the center-line gain was small, amounting to ±1.5%, 3σ over the course of these measurements.

The results are shown plotted in Fig. 49.30. Note the ~20% decline in gain as the "minus" side of the aperture is approached on the horizontal diameter. Note also the ~3% increase in gain on the "plus" side of the amplifier. This is the well-known "cold-side" effect[14] that is characteristic of disk amplifiers having an even number of disks. This effect can be summarized as follows: The two end disks are not evenly pumped across the horizontal axis. The edges of the disks closest to the entrance and exit apertures of the amplifier have only a small solid angle subtended by unfiltered flash lamps and are thus relatively weakly pumped. In an amplifier with an even number of disks, these weakly pumped or "cold" portions of the end disks are both on the same side of the amplifier and therefore add.

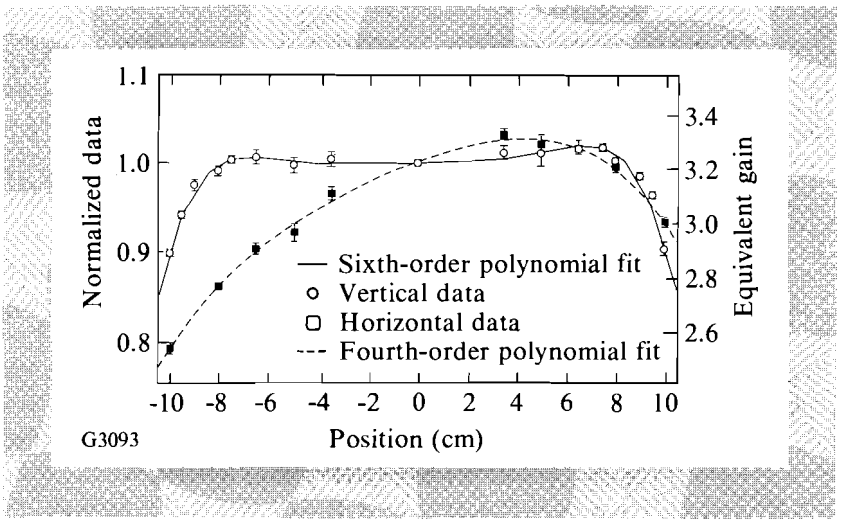

Fig. 49.30
Measured small-signal gain on a horizontal and vertical diameter.

The gain-uniformity goal was ±10% of the center-line gain at any location in the clear aperture. The original center-line gain goal was 3.0. Thus, the goal was to have the gain at any location within the clear aperture be between 2.7 and 3.3. By operating the amplifier at a center-line gain of 3.22, it can be seen from Fig. 49.30 that the small-signal gain at any location within the aperture is in the range of 2.57 to 3.32. Improvements to the gain uniformity, particularly near the edges, have been suggested by pump-light ray tracing performed on the amplifier.

Extensive ray tracing was performed as part of the design of this amplifier. A fully three-dimensional, time-instantaneous, Monte-Carlo ray-trace code[15] was used to model the transport of energy from the flash lamps to the laser disks. Symmetry in the amplifier was used to reduce the ray-tracing problem to only one quadrant of the amplifier. Two million rays at 200 wavelengths were traced in a typical single-quadrant calculation. *S*- and *P*-averaged polarization properties were used. Flash lamps were accurately modeled as volume absorber-emitters using the Trenholme-Emmett-Jancaitis flash-lamp model.[16] Spatial resolution of the energy deposition in the glass was treated by dividing the disks into many volume segments, each of which is assigned the measured absorption spectrum of the Nd:glass. To obtain the actual stored energy at any segment within the model it was only necessary to normalize to the measured center-line stored

energy. Small-signal-gain results are obtained by tracing a fan of rays on either the horizontal or vertical diameters of the clear aperture through the disks using the predicted stored energies in the disk segments to calculate the gain.

The small-signal-gain results on the horizontal diameter are replotted in Fig. 49.31 along with the ray-tracing predictions. Since the ray-tracing results are inherently statistical, they are plotted as a band, which represents the $\pm 1\sigma$ ($\pm 3\%$) confidence limits associated with the results. The agreement is excellent over the majority of the clear aperture. The gain at the very edges of the aperture is sensitive to the details of the ends of the short-(end) pump modules and short-pump-module reflectors. In particular, modeling shows that changing the edges of the short-pump modules from wrapping around the last lamp to a simple 45° angle improves the horizontal gain profile near the edge. It is hypothesized that the edge gain is similarly sensitive to the treatment of the edges of the blast shields and their retainers, which have not been fully included in this model. Inclusion of this detail may result in closer agreement for the end points.

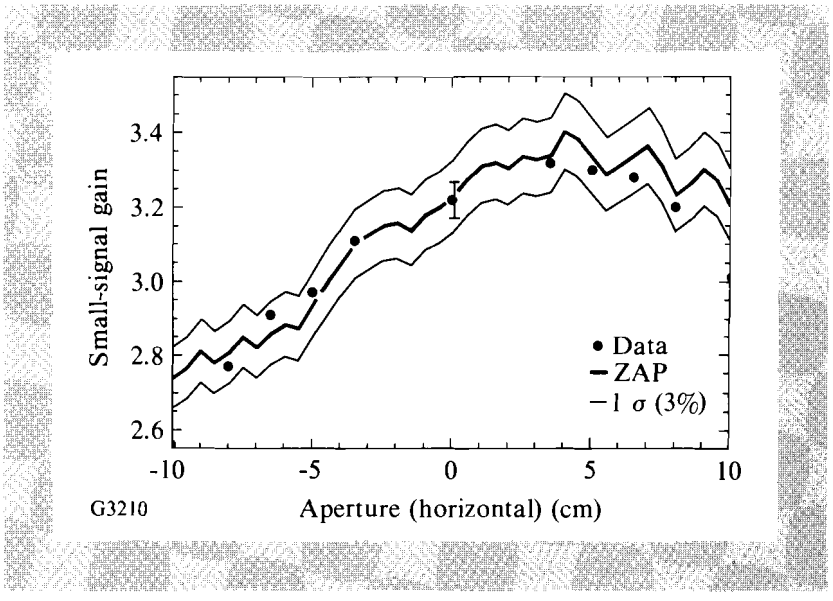

Fig. 49.31
The gain data on a horizontal diameter of Fig. 49.30 replotted along with the ray-tracing predictions. Note that the ray-tracing predictions are plotted as a band representing the $\pm 1\sigma$ confidence limits.

Further detailed examination of the model results for the horizontal diameter confirms that the variation is virtually entirely because of nonuniform pumping of the end disks. The interior disks are uniformly pumped on the horizontal diameter to $\pm 1\%$.

The gain in the vertical direction is very uniform until the edge of the aperture is approached. This is as expected since movement in the vertical direction accesses regions of the end disks at the same distance from the lamps. Variation can only occur close to the edge of the aperture where the glass is "shaded" by the disk holder.

Figure 49.32 replots the vertical-diameter gain data along with the ray-tracing predictions versus radial position. In this plot the upper and lower gain data sets have been averaged together. The ray tracing predicts a "horn" near the edge of

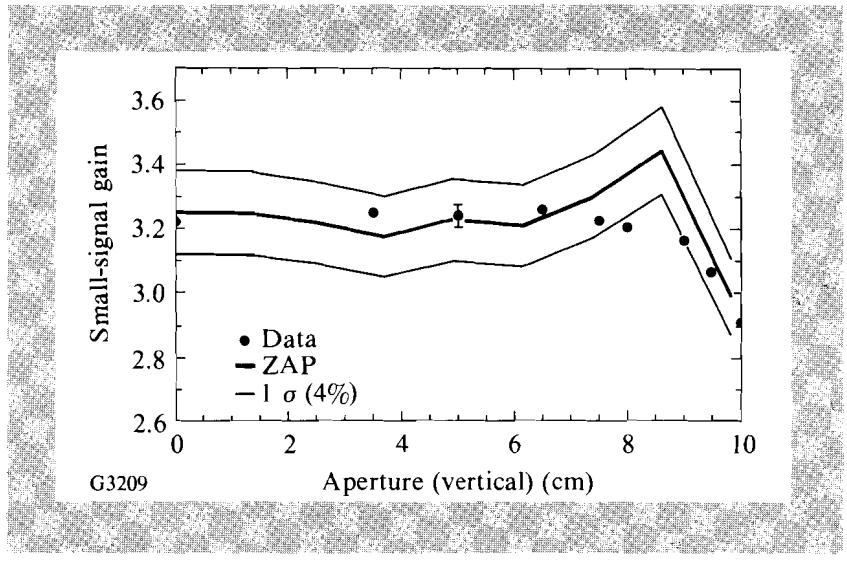

Fig. 49.32
The gain data on a vertical diameter of Fig. 49.30 replotted along with the ray-tracing predictions. Note that the ray-tracing predictions are plotted as a band representing the $\pm 1\sigma$ confidence limits.

the aperture. The data is much more uniform and does not display a similar increase. Further simulations are planned to investigate this.

Also shown on the plots in Fig. 49.30 are a polynomial fit $g_h(x)$ to the horizontal and a polynomial fit $g_v(y)$ to the vertical data. If the gain variation at the very edge of the aperture is assumed to be rotationally symmetric, and is assumed to be accurately represented by the measurements made along the vertical diameter, then an estimate of the gain in the entire aperture can be obtained. Let $g_v(y)$ be the gain measured on the vertical diameter and $g_h(x)$ be the gain measured on the horizontal diameter. Let $g(x,y)$ be the estimated gain at location (x, y) in the aperture. Then

$$g(x,y) = \frac{g_h(x)}{g_v(y)} g_v(r) ,$$

where $r = \sqrt{x^2 + y^2}$ is simply the radius. The function $g(x, y)$ is plotted in Fig. 49.33. If the log of this function is integrated over the total aperture area, the total stored energy in the amplifier may also be estimated. Using a stimulated-emission cross section of 3.5×10^{-20} cm^2, the total stored energy is 3.61 kJ. The storage efficiency η defined by

$$\eta = \frac{\text{total stored energy}}{\text{energy in bank}} = 1.7\% .$$

The small-signal performance of this amplifier meets or exceeds the requirements[17] for the OMEGA Upgrade. It achieved the required stored-energy density of 0.41 J/cm^3. The amplifier exceeded the required storage efficiency of 1.14% with adequate gain uniformity across the aperture.

Large-Signal Gain

To measure its large-signal gain, the amplifier was deployed as an additional final amplifier on one beamline of the OMEGA laser system. The original OMEGA beamline final amplifiers, 9.0-cm-diam rod amplifiers, routinely

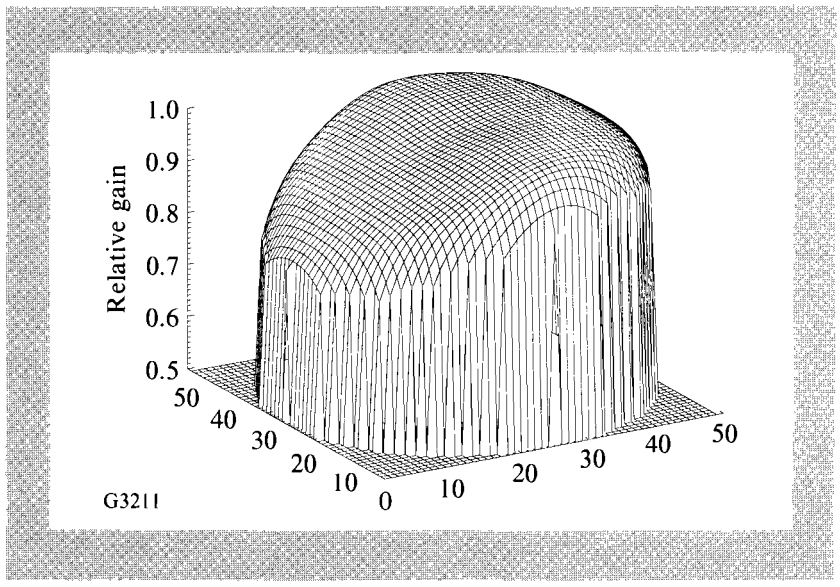

Fig. 49.33
Single-pass, small-signal-gain approximation function versus x-y location in the clear aperture. This gain was averaged over the area occupied by the in-coming and out-going beams in the center of the amplifier. The average gain thus calculated was used as an input for the RAINBOW code.

deliver over 120 J per beam in a 750-ps pulse. Since the disk amplifier is designed to operate with 300 to 350 J of input drive energy, it was necessary to angularly double pass with an input beam of significantly smaller diameter (~16 cm) than the clear aperture (20 cm). Although the beam size is reduced by this technique, the output fluences are comparable to those envisioned for actual use. A schematic of the experimental setup is shown in Fig. 49.34.

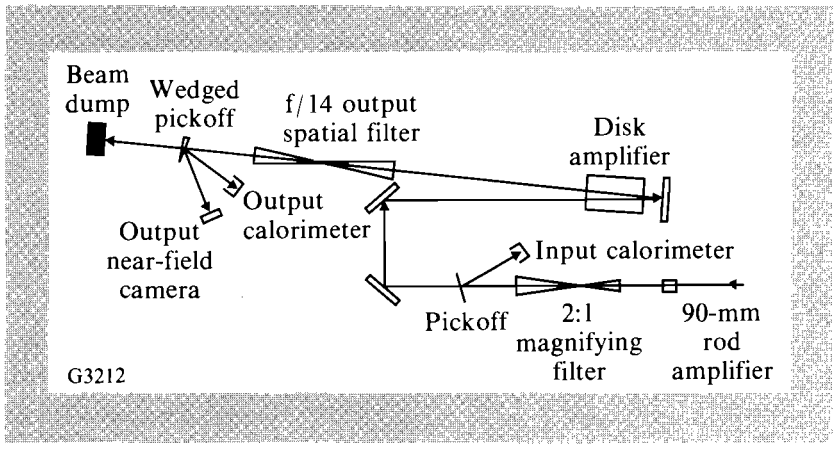

Fig. 49.34
Schematic of the large-signal-gain setup. The output of beamline 6-4 was turned and double passes the amplifier. All output diagnostics are located after the output spatial filter.

The output of beamline 6-4 was reflected to the amplifier by a mirror pair located just after the OMEGA output calorimeter pickoff. This allowed use of the existing OMEGA calorimetry system to measure input energy to the amplifier. This calorimeter was calibrated to read disk-amplifier input energy directly by comparison with a whole-beam calorimeter temporarily placed after the mirror pair. The beam propagates ~14 m from the mirror pair to the amplifier to permit the input and output beams to separate.

The beam was reflected for the second pass through the amplifier by a normal-incidence high reflector placed 73 cm from the corner of the nearest disk. This

resulted in the minimum delay between passes for any part of the amplifier of 4.8 ns. The maximum delay between passes for any part of the amplifier is 15.4 ns. Yarema and Milam[18] demonstrated only a small change in the saturation fluence with a pulse-width change of 1.4 to 20 ns. Since the delays between passes for any part of the amplifier fall within this range, lower lasing-level relaxation effects can be ignored in modeling this configuration.

The output beam propagated ~15 m to a 3-m focal length, 1:1 magnification spatial filter. For all of the tests performed, the cutoff half-angle in this filter was 400 μrad. All output diagnostics were located after the spatial filter (refer to Fig. 49.34). The second surface reflection from a wedge was used for the output calorimeter. The first surface reflection was used for output-beam, near-field photography.

All large-signal gains were measured with the amplifier at 80% of nominal capacitor-bank energy. The chosen bank energy corresponded to a center-line, small-signal gain of approximately 3.22. Three series of measurements were made, each with different beam spectral characteristics: transform-limited 740-ps pulses, 5-Å-bandwidth, FM-modulated 740-ps pulses, and angularly dispersed, frequency-modulated (SSD),[19] 740-ps pulses. Each "measurement" in one of the series actually consisted of three separate submeasurements. The first was an OMEGA shot to take a near-field photograph of the input beam at the requested drive energy. This measurement could not be made simultaneously with the gain measurement by use of a pickoff because of the resulting low-energy density on the film. The second submeasurement was of the actual input and output energies with the amplifier firing. The third submeasurement was of the input and output energies with the amplifier not fired in order to monitor the passive transmission of the entire stage including the mirrors and spatial filter. This yielded the transmission of the stage for use in modeling and served as a check for any possible misalignments.

The results of the first series with conventional transform-limited pulses is shown in Fig. 49.35. The actual data points are shown as crosses. The error bars in the vertical direction are the $\pm 3\sigma$ ($\pm 1.5\%$) confidence limits associated with the output calorimeter. The error bars in the horizontal direction are the $\pm 3\sigma$ confidence limits associated with the input calorimeter. Data extends up to an output energy of just over 700 J, corresponding to an output fluence (normal to the beam) of 3.5 J/cm^2. The maximum output fluence contemplated for this amplifier in the OMEGA Upgrade is 4.0 J/cm^2.

Also shown on this plot are the predictions of the laser energy-transport code RAINBOW.[20] This azimuthally-symmetric ray-tracing code features a modified Frantz-Nodvik[21] treatment of gain saturation that includes linear absorption in the laser glass and the saturation fluence model of Martin and Milam.[22] The required inputs to the model are the small-signal gain, the passive losses, the input beam fluence, and the saturation fluence.

The small-signal gain was measured during each gain shot by double passing a cw probe beam from the previously described small-signal-gain apparatus through the amplifier at a high angle so that the probe-beam collection optics did

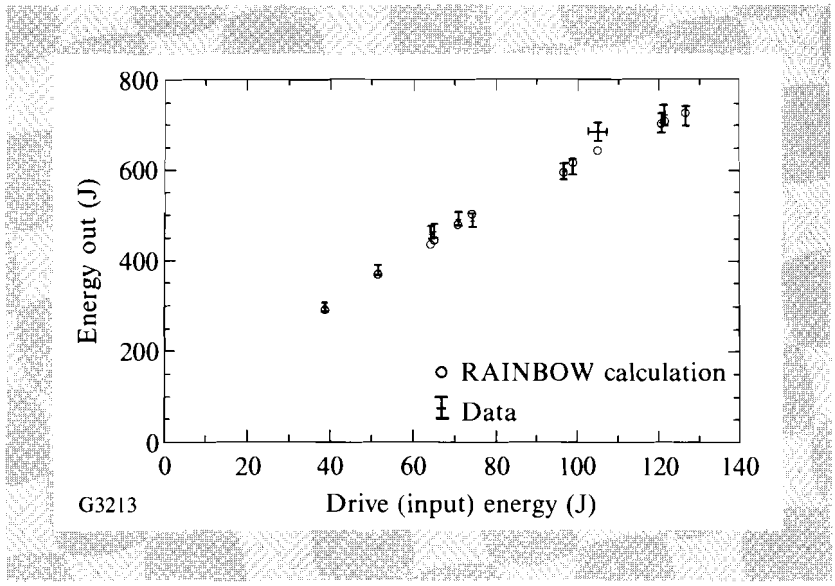

Fig. 49.35
Double-pass output energy in joules versus input drive energy in joules for transform-limited pulses. The open circles are the RAINBOW predictions.

not intercept the extracting beam. This not only allowed monitoring of the small-signal gain on each shot but also allowed verification of the timing of the extracting pulse relative to the temporal gain profile by observation of the gain saturation. The gain measured this way was corrected by a known ratio to yield the equivalent center-line-measured, small-signal gain. This center-line gain was used to normalize the spatial plot of gain shown in Fig. 49.33. A spatial average was then taken over an area equal to that of the overlapped beams in the center of the amplifier. This spatially averaged, small-signal gain was then used as input to the code for each simulation.

Since the passive losses were not expected to change over the course of the experiment (the alignment was left undisturbed), the average of all the transmission measurements was used to compute a single passive loss of the stage. The stage included the double-passed amplifier, three mirrors, and the output spatial filter. This loss was used for all simulations. The average passive loss for the stage was measured to be 0.937±0.023. In the simulations, this loss was distributed through the amplifier as a 0.00226 cm^{-1} loss. Approximately 1/3 of this loss may be attributed to the actual base-glass absorption, which is specified to be less than 0.0015 cm^{-1} at 1.05 μm per disk. The remainder is hypothesized to be caused by birefringence and scattering losses. The passive transmission in double pass for the entire stage is greater than the specified passive transmission for the amplifier alone (0.96) squared to account for double passing, 0.922.

The input beam fluences were deduced from the input calorimetry and the near-field photographs of the OMEGA output taken at the same energy. The film[23] data was digitized and density-to-intensity corrected by use of a separately generated D-log(I) curve for the same pulse width and wavelength. The average intensity $< I >$ on the film was calculated by

$$< I > = \int_0^\infty I \frac{dE}{dI}\, dI \Big/ \int_0^\infty \frac{dE}{dI}\, dI \ .$$

where dE/dI is the fraction of energy in the intensity range dI at the intensity I. The average beam-fluence (F_{avg}) input to the code was then calculated from

$$F_{avg} = \tau < I > ,$$

where τ is the temporal pulse width. Since dE/dI is not a delta function in the input near fields because of both beam modulation and the not-infinitely-steep beam edges, the simulations were all performed with an 18th-order superGaussian beam-edge profile to better approximate the actual beam shape. A perspective plot of a typical input near field that has been density-to-intensity converted is shown in Fig. 49.36.

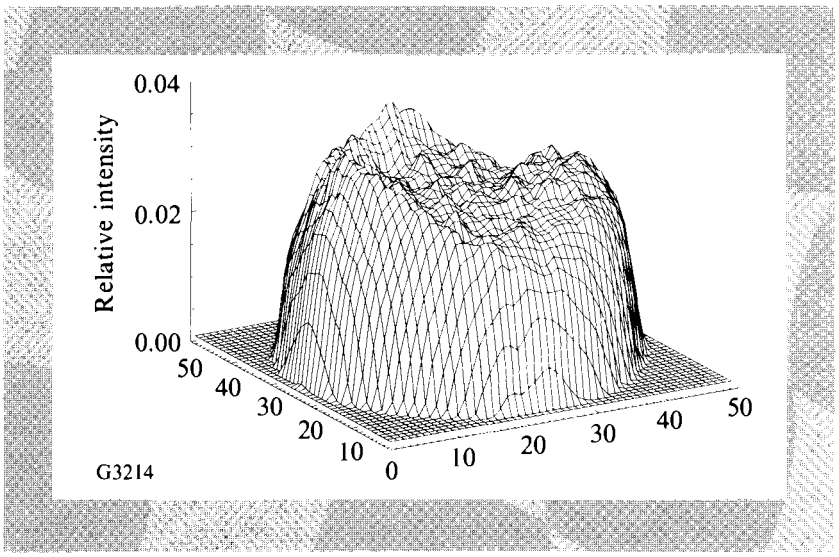

Fig. 49.36
Perspective plot of a density-to-intensity converted near field taken at the input to the amplifier. The z axis is relative intensity and the x and y axes are relative position. The input pulse is very nearly flat-topped. This is a transform-limited pulse with 51.2-J energy.

The saturation fluence F_{sat} is a function of both the glass type and the total fluence. All four disks were of phosphate glass; two were of Hoya[24] LHG-8 and two of Schott[25] LG-750. These two glass types have similar lasing properties. The saturation fluence for these glasses has been measured to be a function of the extracting fluence. This effect is caused by the inhomogeneous broadening of the ${}^4F_{3/2}$ to ${}^4I_{11/2}$ transition. A simplified explanation is as follows: The Nd^{+3} ions have some cross section and central wavelength distribution. The ions with a larger cross section and better wavelength match to the extracting beam are more readily depleted. The remaining ion population has a lower effective cross section and is a poorer spectral match resulting in a higher saturation fluence. The most recent saturation fluence data for these glass types is that of Yarema and Martin[18]

$$LHG-8\text{: } F_{sat} = 3.38 + 0.555 \ln(F_{out}) \text{ J/cm}^2$$
$$LG-750\text{: } F_{sat} = 3.88 + 0.313 \ln(F_{out}) \text{ J/cm}^2 ,$$

where F_{out} is the output fluence of their amplifiers that had small-signal gains of 4 to 5. For this work, a computationally simpler form based on fits to earlier 1-ns data[22] for LHG-8 was used for both glass types:

$$F_{\text{sat}}(t) = 3.75 + 0.032 \int_{-\infty}^{t} I(t')dt' \text{ J/cm}^2 ,$$

where t is the time of the current photon.

In Fig. 49.35, with the exception of three data points, all RAINBOW predictions fall within the error bars of the measurement. Considering the number of approximations inherent in the simulations this agreement is excellent. In the three exceptions, the code estimates are conservative, which is desirable in a design tool. RAINBOW also calculates the maximum ΔB through the stage. The maximum calculated ΔB for all three series occurred on the 720-J output shot and was 0.89 rad. This is the same value that is anticipated for actual use on the OMEGA Upgrade.

In the second series of measurements, an FM modulation was applied to the 740-ps pulse using an electro-optic modulator.[26] The resulting bandwidth consisted of a 5 Å "comb" of sidebands each separated by 9.65 GHz. The 5-Å bandwidth is of the same order as the 7.5-Å bandwidth planned for the OMEGA Upgrade.[27] Reduction in the large-signal gain because of a decrease in the small-signal gain experienced by the wings of the spectrum is not expected since the 5-Å bandwidth is small compared to both the fluorescence linewidth of these glasses (~230 Å) and the 3-db-gain bandwidth of the amplifier in double pass (~100 Å). No increase in extraction is expected because of the increased bandwidth of the extracting beam accessing more of the inhomogeneously broadened line since the 5-Å bandwidth is small compared to the homogeneous linewidth[28] (~24 Å for LG-750, LHG-8 expected to be similar).

The results of the second series of measurements are shown in Fig. 49.37. Again, output energy is plotted versus drive energy in joules. Also shown again are the RAINBOW simulations. All of the predictions fall within the error bars

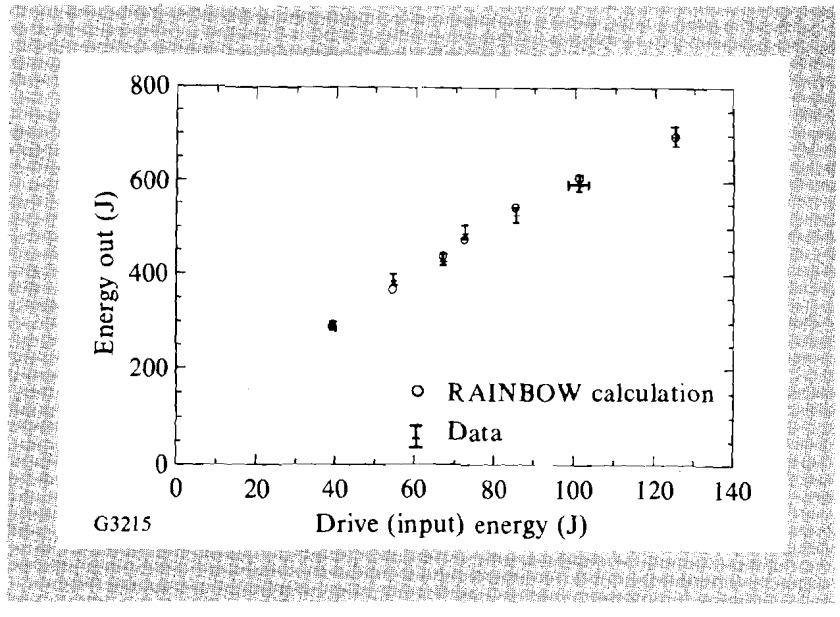

Fig. 49.37
Double-pass output energy in joules versus input drive energy in joules for FM-modulated pulses. The open circles are RAINBOW predictions for transform-limited pulses of the same energy. The differences between predictions that do not take into account bandwidth and the data are within the error bars of the measurement. This is as expected because the FM bandwidth is still small relative to the published homogeneous linewidth of LG-750. LHG-8's homogeneous linewidth is expected to be similar, because of the similarity in glass composition.

of the measurement. Since bandwidth has been ignored in these simulations it may be concluded that within the error bars of these measurements, 5-Å-FM bandwidth has no effect on the large-signal gain of this amplifier.

The third and final series of measurements were made with spatially-dispersed, FM-modulated (SSD), 740-ps pulses. The same FM modulator was used as in the previous series. A grating after the modulator angularly disperses the FM-modulated light by 67 μrad/Å in the vertical direction at the amplifier stage. Data in this series were limited to drive energies <75 J because of the low diffraction efficiency of the prototype grating used as the dispersing element. In addition, the near-field beam quality was degraded because of grating imperfections. The results are shown in Fig. 49.38 along with the RAINBOW simulations. The three predictions underestimate the output energy, one significantly. This is attributed to a low, small-signal-gain measurement caused by poor utilization of the range of the *A*-to-*D* converters in the digitizing oscilloscopes. No effect on energy transport can be attributed to the spatial dispersion.

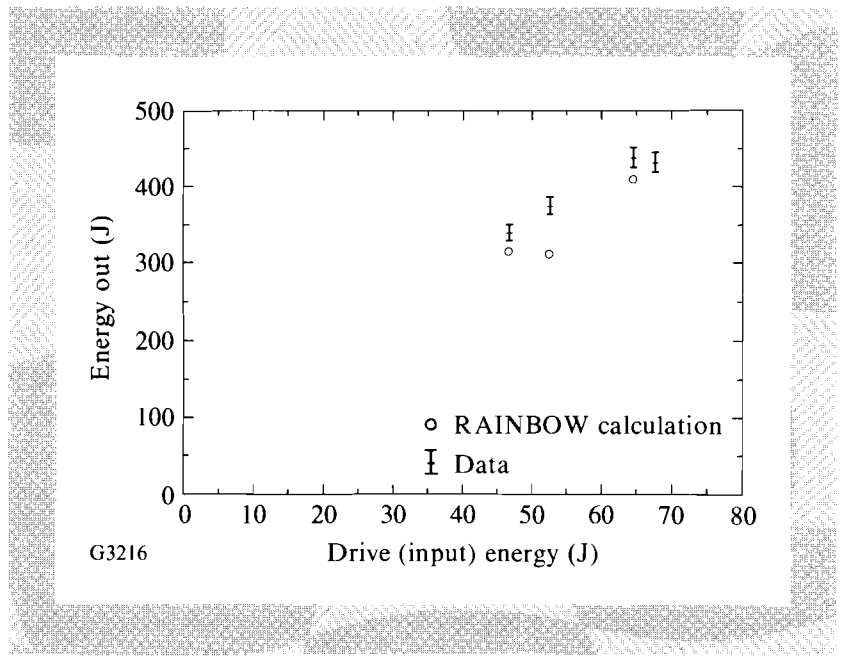

Fig. 49.38
Double-pass output energy in joules versus input drive energy in joules for spatially dispersed FM-modulated pulses. The open circles are RAINBOW predictions for transform-limited pulses of the same energy.

Conclusion

The OMEGA Upgrade will use a modern, 20-cm clear aperture, Nd:glass Brewster-disk amplifier as the final amplifier. This device has been designed, constructed, characterized, and it has met or exceeded its design goals in all aspects of energy transport. These goals are summarized in Table 49.V. Specifically, it achieved a small-signal gain of 3.22 at only 80% of design bank energy with a storage efficiency of 1.7%. Passive losses are consistent with the values assumed for the OMEGA Upgrade. The amplifier has been tested in the large-signal regime by double passing at a pulse width of 740 ps. It produced over 720 J of energy with 126-J drive at an output fluence of 3.5 J/cm^2. Wavefront characterization results will be presented in a future article.

Table 49.V: 20-cm-disk amplifier performance.

	Goal	Achieved
Center-line small-signal gain	3.0	3.22
(at) bank energy	300 kJ	240 kJ
Gain G uniformity at center-line gain G_{CL}	$2.7 < G < 3.3$ $G_{CL} = 3.00$	$2.57 < G < 3.32$ $G_{CL} = 3.22$
Storage efficiency	1.14%	1.7%
Passive transmission	0.922 double pass amplifier only	0.937 double pass entire stage
Output energy	1050 J	730 J drive limited
(at) max output fluence	4.0 J/cm^2	3.5 J/cm^2 drive limited

G3230

ACKNOWLEDGMENT

This work was supported by the U.S. Department of Energy Office of Inertial Confinement Fusion under agreement No. DE-FC03-85DP40200 and by the Laser Fusion Feasibility Project at the Laboratory for Laser Energetics, which is sponsored by the New York State Energy Research and Development Authority and the University of Rochester.

REFERENCES

1. We are grateful for the cooperation of our colleagues at Lawrence Livermore National Laboratory; especially Dr. H. T. Powell, Dr. J. E. Murray, and Dr. A. T. Erlandson.
2. Rutherford Appleton Laboratory Annual Report to the Laser Facility Committee, pp. A6.6–A6.12, (1985).
3. S. M. Yarema and J. E. Murray, Lawrence Livermore National Laboratory Laser Program Annual Report 1980, UCRL 50021-80 (1981), pp. 2-234–2-244.
4. Private communication from K. Moncur, KMS Fusion, Inc., 1989.
5. Lawrence Livermore National Laboratory Laser Program Annual Report 1986, UCRL 50021-86 (1987), pp. 4-14–4-59.
6. LLE Review **44**, 205 (1990).
7. M. J. Shoup III, J. H. Kelly, M. M. Tedrow, F. A. Rister, and K. Thorp, "Mechanical Design of 15- and 20-cm Clear Aperture Disk Amplifiers for the OMEGA Upgrade," presented at the *SPIE's OE-LASE '92 Technical Conference on High-Power Lasers*, Los Angeles, CA, 20–25 January 1992.

8. M. Andre *et al.*, "High Energy Laser System Development at 'Centre D'Etudes de Limeil' in France," presented at the *IAEA Technical Committee Meeting on Drivers for Inertial Confinement Fusion*, Osaka, Japan, 15–19 April 1991.

9. Dr. J. E. Murray of Lawrence Livermore National Laboratory developed this technique.

10. Tektronix Inc., Beaverton, Oregon, USA. Reference to a company or a product name does not imply approval or recommendation of the product by the University of Rochester or the U.S. Department of Energy.

11. R. B. Blackman and J. W. Tukey, *The Measurement of Power Spectra,* in *The Point of View of Communications Engineering* (Dover Publications, New York, 1958).

12. Dr. K. Jancaitis of Lawrence Livermore National Laboratory modeled the parasitic characteristics of these disks prior to their fabrication and predicted that there would be no self-oscillation.

13. LLE Review **37**, 16 (1988).

14. J. E. Murray, H. T. Powell, and B. W. Woods, "Optimized Flash-lamp Pumping of Disc Amplifiers," presented at *SPIE's OE/LASE '86 Conference*, Los Angeles, CA, 19–24 January 1986. Available as preprint UCRL-93321 from Technical Information Department, Lawrence Livermore National Laboratory, P.O. Box 808, Livermore, CA 94550.

15. The code used is a greatly updated and enhanced version of the code ZAP originally written by Systems, Science and Software for the Naval Research Lab by J. H. Alexander, M. Troost, and J. E. Welch, ARPA order number 660, Contract number N00014-70-C-0341, 1971.

16. K. S. Jancaitis and H. T. Powell, "An Empirical Model for Predicting the Absolute Radiative Emission and Absorption Spectra of Xenon Flash Lamps." Available as preprint UCID-21226 from Technical Information Department, Lawrence Livermore National Laboratory, P.O. Box 808, Livermore, CA 94550.

17. R. S. Craxton, Ed., *OMEGA Upgrade Preliminary Design*, Laboratory for Laser Energetics Report DOE/DP 40200-101, University of Rochester, pp. 6.28–6.30, 1989. Note that the performance numbers in this document are based on the earlier value for the stimulated-emission cross section of 4.0×10^{-20} cm^2.

18. S. M. Yarema and D. Milam, IEEE J. Quantum Electron. **18**, 1941 (1982).

19. S. Skupsky, R. W. Short, T. Kessler, R. S. Craxton, S. Letzring, and J. M. Soures, J. Appl. Phys. **66**, 3456 (1989).

20. D. C. Brown, "Simulation and Modeling of Small-Scale Self-Focusing Effects," in *High-Peak-Power Nd:Glass Laser Systems* (Springer-Verlag, New York, 1981), Sec. 7.7, p. 229.

21. L. M. Frantz and J. S. Nodvik, J. Appl. Phys. **34**, 2346 (1963).

22. W. E. Martin and D. Milam, IEEE J. Quantum Electron. **18**, 1155 (1982).

23. The film used was Kodak type 4143 IR film. Reference to a company or a product name does not imply approval or recommendation of the product by the University of Rochester or the U.S. Department of Energy.

24. Hoya Optics, Inc., 3400 Edison Way, Fremont, CA 94538-6190. Reference to a company or a product name does not imply approval or recommendation of the product by the University of Rochester or the U.S. Department of Energy.

25. Schott Glass Technologies, Inc., 400 York Avenue, Duryea, PA 18642. Reference to a company or a product name does not imply approval or recommendation of the product by the University of Rochester or the U.S. Department of Energy.

26. LLE Review **37**, 29 (1988).

27. R. S. Craxton, Ed., *OMEGA Upgrade Preliminary Design*, Laboratory for Laser Energetics Report DOE/DP 40200-101, University of Rochester, pp. 3.21–3.24, 1989.

28. D. W. Hall, M. J. Weber, and R. T. Brundage, J. Appl. Phys. **55**, 2642 (1984).